Turbulent properties of the solar wind within corotating interaction regions: superposed epoch analysis of simulations and observations

Keyvan Ghanbari [1] Vladimir Florinski [1] Gary P. Zank [1]

[1]Department of Space Science, Center for Space Plasma and Aeronomic Research (CSPAR), The University of Alabama in Huntsville

THE UNIVERSITY OF ALABAMA IN HUNTSVILLE

CENTER FOR SPACE PLASMA AND AERONOMIC RESEARCH AND THE DEPARTMENT OF SPACE SCIENCE

Introduction

The solar wind contains fluctuations over a broad range of spatial and temporal scales that are commonly referred to as "turbulence". In-situ observations from *Mariner*, *Helios*, *Ulysses* , many spacecraft and very recently *Parker solar probe* (PSP) have collected valuable information on the state and spatiotemporal evolution of turbulence in the outermost regions of the solar corona up to further distances from Sun. Turbulence plays a significant role in various aspects of plasma behavior in space including solar wind acceleration, solar energetic particle transport, plasma heating, and galactic cosmic ray (GCR) modulation [1].

The solar wind is comprised of plasma streams with different radial velocities, but is primarily bimodal (i.e., either "fast" or "slow"). Fast streams originate from open interplanetary magnetic field (IMF) lines in the high latitude regions on the Sun, while slow streams originate from the solar equatorial regions. The turbulent properties, such as the fluctuation energy and the correlation length, are also different between fast and slow solar-wind regimes [1]. Owing to solar rotation, these regimes interact and form more complex structures in terms of the topology of the IMF and plasma features. The most common of these are corotating interaction regions or CIRs. A CIR is generated in the solar wind when a fast stream overtakes the foregoing slow wind [3]. A shear layer between the fast and slow wind within a CIR is categorized as a tangential discontinuity (TDs) and is called a stream interface (SI).

The model presented in this poster is based on a 3D magnetohydrodynamic (MHD) simulation of the solar wind plasma and bulk turbulence properties. The simulations were conducted using partially assumed and partially data-driven physical geometry and boundary conditions to generate CIRs in the heliocentric distances between 0.3 and 5 au. The entire physical domain can be covered by a single model because the inner boundary is well outside the Alfvén critical point (~ 10 R_s). The model presented here offers several advantages over previous work.

- The dynamic inner boundary condition is an improvement that enables us to generate CIRs that are reasonably comparable with observations.
- The turbulence system of equations is being solved for six turbulent quantities in three dimensions allows us to investigate the variations of each quantity within a CIR.
- The model does not use a parametric source term to describe in situ turbulence production by shear, relying instead on the enhancement of pre-existing turbulence according to the transport equation.

Theory and Methods, part 1

Framework: The underlying numerical framework is based on a three-dimensional geodesic mesh consisting of a 2D hexagonal tesselation extruded radially in a concentric fashion with a variable stepping. A detailed description of the framework can be found in [6]. The background component of the model solves the standard system of MHD conservation laws for the flow density, momentum and energy, and magnetic flux. The system of MHD equations is solved with a finite volume second-order (space and time) method on hexagonal prisms [6]. Reconstruction is employed to achieve second-order accuracy using one- and two-dimensional versions of the weighted essentially non-oscillatory (WENO) limiter in both radial and tangential directions. Fluxes are computed using the HLLC Riemann solver.

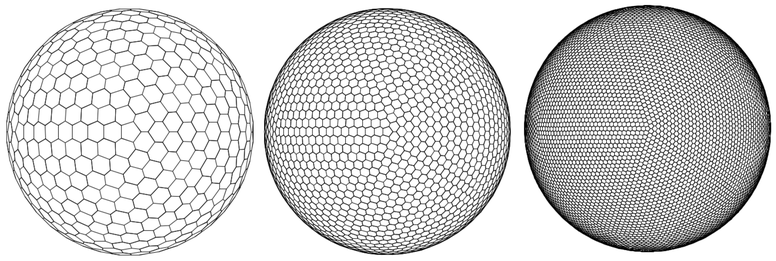

Figure 1. Samples of geodesic grids of level 3 (left), 4 (middle) and 5 (right).

Bouundary Condition: The Wilcox solar observatory [wso.sstanford.edu] (WSO) provides coefficients of the Legendre expansion for the potential field source surface (PFSS) model for all recorded Carrington rotations (CR) from 1976 until the present time up to the ninth degree harmonic. By constructing surface magnetic field maps from the Legendre expansion at ($R = 2.5R_s$) the inner boundary of the simulation is set up with given fast and slow streams and current sheet identified as the zone where the polarity of the magnetic field switches sign. Coefficients of the years 2007 and 2008 were used in this simulation.

2 Samples of reconstructed maps are shown in firgure 2. In this maps Blue regions has negative polarity (field is inwards to the sun), yellow and red regions has positive polarity (outward from the sun). The **gray area** is taken to be the **slow streams** and colored area is fast stream.

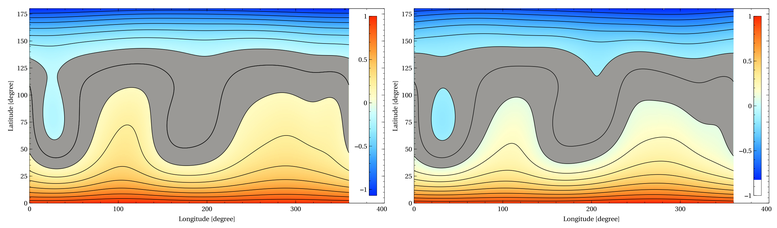

Figure 2. Magnetic polarity (blue: negative and red: positive) and slow (gray)-fast (colored) stream maps for carrington rotaions 2051 and 2052 implemented in the simulation.

This method enables us to generate island shaped regions in the inner boundary of our simulation. Such an island has fast stream features while the surounding regions has slow streams features.

Theory and Methods, part 2

Modelling: The turbulence model is based on the six-equation formalism of [10] that consists of equations for the densities of energy-like quantities and the correlation lengths. The energy variables are the energy sum E_t, the cross-helicity H_c and the energy difference E_d. We use the turbulence transport equations in a quasi-conservative form, where the transported quantities have the units of energy density, and the fluxes describe advection with the solar wind; the remaining terms describing coupling with the large-scale flows are treated as source terms. The form of the turbulence transport equations that are implemented in the model is slightly different from those of [10]. We use only "extensive" variables that correspond to the energy densities and integrals times the plasma density, ρE_t, ρH_c, ρE_d, $\rho L_{\pm}$, and ρL_d. The evolution equations are given as

$$\frac{\partial(\rho E_t)}{\partial t}+\nabla\cdot(\rho\mathbf{u}E_t) = -\frac{1}{2}(\nabla\cdot\mathbf{u})\rho E_t - M\rho E_d - \alpha\rho\left[\frac{(E_t+H_c)^2(E_t-H_c)^{1/2}}{L^+}+\frac{(E_t-H_c)^2(E_t+H_c)^{1/2}}{L^-}\right], \quad (1)$$

$$\frac{\partial(\rho H_c)}{\partial t}+\nabla\cdot(\rho\mathbf{u}H_c) = -\frac{1}{2}(\nabla\cdot\mathbf{u})\rho H_c - \alpha\rho\left[\frac{(E_t+H_c)^2(E_t-H_c)^{1/2}}{L^+}-\frac{(E_t-H_c)^2(E_t+H_c)^{1/2}}{L^-}\right], \quad (2)$$

$$\frac{\partial(\rho E_d)}{\partial t}+\nabla\cdot(\rho\mathbf{u}E_d) = -\frac{1}{2}(\nabla\cdot\mathbf{u})\rho E_d - M\rho E_t - \alpha\rho E_d\left[\frac{(E_t+H_c)^{3/2}}{L^+}+\frac{(E_t-H_c)^{3/2}}{L^-}\right], \quad (3)$$

$$\frac{\partial(\rho L^{\pm})}{\partial t}+\nabla\cdot(\rho\mathbf{u}L^{\pm}) = -\frac{1}{2}(\nabla\cdot\mathbf{u})\rho L^{\pm} - \frac{M}{2}\rho L_d, \quad (4)$$

$$\frac{\partial(\rho L_d)}{\partial t}+\nabla\cdot(\rho\mathbf{u}L_d) = -\frac{1}{2}(\nabla\cdot\mathbf{u})\rho L_d - M\rho(L^+ + L^-), \quad (5)$$

where the mixing term is $M = (\nabla\cdot\mathbf{u})/2 - \hat{\mathbf{b}}\cdot(\hat{\mathbf{b}}\cdot\nabla)\mathbf{u}$, where $\hat{\mathbf{b}} = \mathbf{B}/B$. Karman–Taylor constant α that is generally thought to be of order one (e.g. [4, 2]). However, in this model $\alpha = 0.05$ because larger values resulted in correlation lengths an order of magnitude larger than expected based on the observations, in agreement with the same conclusion reached by [8]. The nonlinear terms are all modeled as in [10] except for the residual energy, which is based on [9].

Results (part 1)

The results of this simulation for solar wind turbulent properties are given in figure 3 with observations (red) and simulation results (blue). The key points for these results are as follows:

- Although reproducing the observations was not our main goal in this simulation, there is a good correspondence in magnitude and the trend of the variations of the turbulent properties.
- The height of the peaks for turbulent energy at the stream interface of the simulated CIRs is shorter than the strong sharp peaks in observations.
- A smaller correlation length is reproduced in slow wind and it is increased in fast wind with a magnitude of about 10^{-2} au. The trend is very similar to the observations.
- Normalized cross helicity is a representation of the heliospheric current sheet crossing at 1 au. There are some inconsistencies caused by transient events such as magnetic islands in the solar wind.
- Simulation results for $\kappa_{\perp/||}$ show the roughly reverse behavior of the two coefficients near CIRs. $\kappa_{\perp}$ is from the order of 10^{20} $cm^2.s^{-1}$ and higher in the fast wind than the slow wind with a valley at the stream interface, while $\kappa_{||}$ is about 10^{22} $cm^2.s^{-1}$ and has an almost reverse trend. The $\lambda_{\perp/||}$ are from the order of 10^{-3} and 10^{-1} au, respectively.

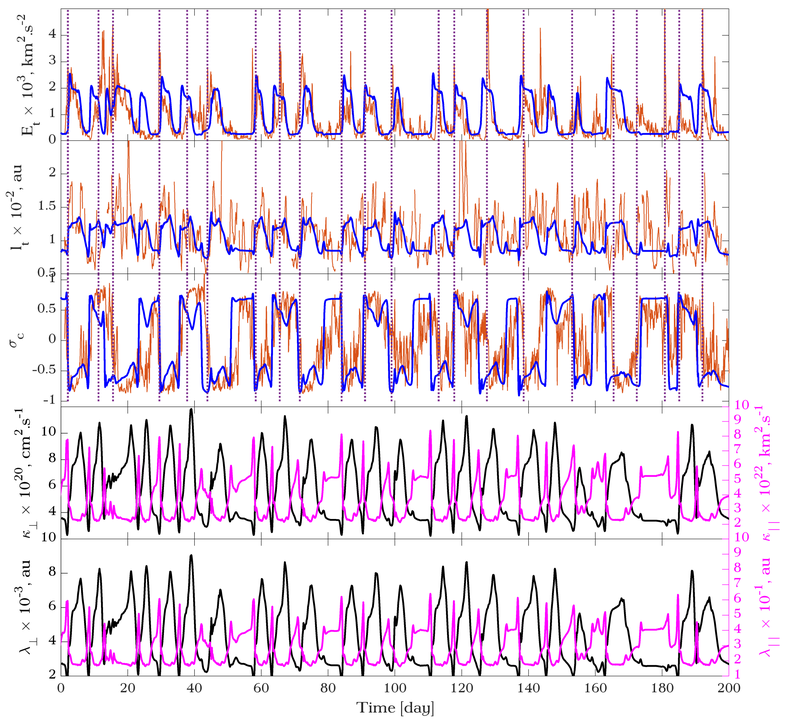

Figure 3. Solar wind turbulence properties during the first 200 days of the year 2007, observation (red) and simulation (blue). From top, E_t, l_t, σ_c, $\kappa_{\perp(black)/||(magenta)}$, $\lambda_{\perp(black)/||(magenta)}$.

Result (part 2)

A spherical slice of the simulation results for E_t (left) and l_t (right) is shown in figure 4. E_t is enhanced at the stream interface of the CIR shown in a red closed curve.

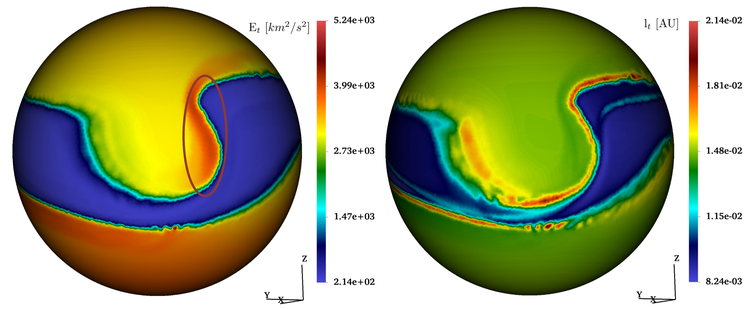

Figure 4. Spherical slice of the simulation results for E_t (left) and l_t (right) at 1 au. Red curve shows a CIR in the simulation.

The superposed epoch analysis (SPE) is performed on both observations (red) and simulation results (blue) of the turbulent properties shown in figure 5. diffusion coefficients are computed for 4 different energies of 100, 200, 500 Mev, and 1 Gev galactic cosmic rays.

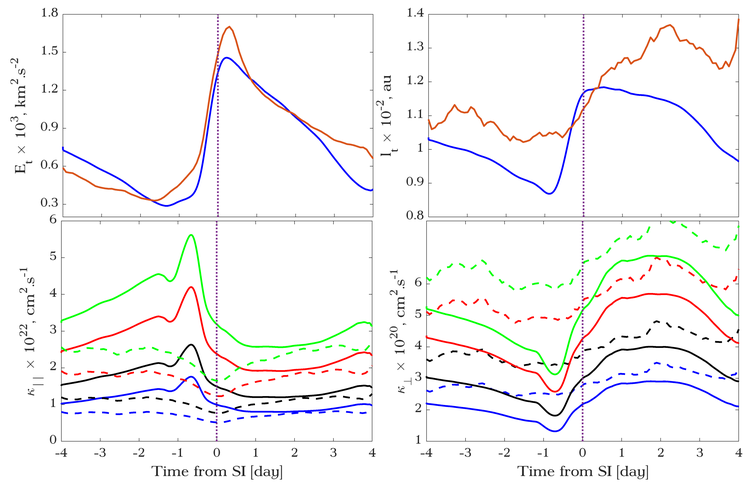

Figure 5. Superposed epoch analysis of the simulation results (blue/solid) versus observations (red/dashed) for E_t (top left), l_t (top right), $\kappa_{||}$ (bottom left) and $\kappa_{\perp}$ (bottom right) for energies 100 (blue), 200 (black), 500 (red) MeV and 1 GeV (green).

- The magnitude and trend of the SPE of the observed turbulent energy near CIRs are well reproduced in the SPE analysis of the simulation results. The peak in E_t is around 1500 $km^2.s^{-2}$ is almost equal to the SPE of the observations.
- The SPE of the correlation length for simulation results is % 10 smaller than that of the observations before and after the stream interface.
- The SPE of the $\kappa_{||}$ is % 10 greater in the slow wind in simulation results compared to the observed SPE values. But it has similar values in fast stream.
- There is a peak at the SPE of the $\kappa_{||}$ for all energies right before the stream interface that is caused by the smaller value of the slab components of the turbulence in the simulation compared to the observations. $\kappa_{||}$ is inversely related to this parameter in the quasi-linear theory framework which is the reference theory for this work.
- The $\kappa_{\perp}$ is also % 10 smaller in simulation results compared to the SPE of the observations. The trends for the observation and simulation results are fairly in agreement with each other.

References

[1] R. Bruno and V. Carbone. The solar wind as a turbulence laboratory. *Living Reviews in Solar Physics*, 10(1):2, 2013.

[2] R. Chhiber, A. V. Usmanov, W. H. Matthaeus, and M. L. Goldstein. Large-scale Structure and Turbulence Transport in the Inner Solar Wind: Comparison of Parker Solar Probe's First Five Orbits with a Global 3D Reynolds-averaged MHD Model. *The Astrophysical Journal*, 923(1):89, Dec. 2021.

[3] N. U. Crooker, J. T. Gosling, V. Bothmer, R. J. Forsyth, P. R. Gazis, A. Hewish, T. S. Horbury, D. S. Intriligator, J. R. Jokipii, J. Kóta, A. J. Lazarus, M. A. Lee, E. Lucek, E. Marsch, A. Posner, I. G. Richardson, E. C. Roelof, J. M. Schmidt, G. L. Siscoe, B. T. Tsurutani, and R. F. Wimmer-Schweingruber. CIR Morphology, Turbulence, Discontinuities, and Energetic Particles.

[4] T. de Karman and L. Howarth. On the Statistical Theory of Isotropic Turbulence. *Proceedings of the Royal Society of London Series A*, 164(917):192–215, Jan. 1938.

[5] A. Dosch, L. Adhikari, and G. P. Zank. The transport of low-frequency turbulence in astrophysical flows: Correlation lengths. In G. P. Zank, J. Borovsky, R. Bruno, J. Cirtain, S. Cranmer, H. Elliott, J. Giacalone, W. Gonzalez, G. Li, E. Marsch, E. Moebius, N. Pogorelov, J. Spann, and O. Verkhoglyadova, editors, *Solar Wind 13*, volume 1539 of *American Institute of Physics Conference Series*, pages 155–158, June 2013.

[6] V. Florinski, X. Guo, D. S. Balsara, and C. Meyer. Magnetohydrodynamic Modeling of Solar System Processes on Geodesic Grids. *The Astrophysical Journal*, 205(2):19, Apr. 2013.

[7] G. M. Mason and T. R. Sanderson. CIR Associated Energetic Particles in the Inner and Middle Heliosphere.

[8] A. V. Usmanov, W. H. Matthaeus, M. L. Goldstein, and R. Chhiber. The Steady Global Corona and Solar Wind: A Three-dimensional MHD Simulation with Turbulence Transport and Heating. *The Astrophysical Journal*, 865(1):25, Sept. 2018.

[9] G. P. Zank, L. Adhikari, P. Hunana, D. Shiota, R. Bruno, and D. Telloni. Theory and transport of nearly incompressible magnetohydrodynamic turbulence. *The Astrophysical Journal*, 835(2):147, jan 2017.

[10] G. P. Zank, A. Dosch, P. Hunana, V. Florinski, W. H. Matthaeus, and G. M. Webb. The Transport of Low-frequency Turbulence in Astrophysical Flows. I. Governing Equations. *The Astrophysical Journal*, 745(1):35, Jan. 2012.

Keyvanghanbari@gmail.com / kg0055@uah.edu

Cramer Hall 2079, Huntsville, AL 35899